(17) B. DasSarma and J. C. Bailar, Jr., *J. Am. Chem. Soc.*, **77**, 5476 (1955).
(18) G. H. McIntyre, Jr., B. P. Block, and W. C. Fernelius, *J. Am. Chem. Soc.*, **81**, 529 (1959).
(19) M. Ciampolini, P. Paoletti, and L. Sacconi, *J. Chem. Soc.*, 2994 (1961).
(20) H. B. Jonassen, G. G. Hurst, R. B. LeBlanc, and A. W. Meibohm, *J. Phys. Chem.*, **56**, 16 (1952).
(21) Reference 11, p 504.
(22) S. M. Nelson and T. M. Shepherd, *J. Chem. Soc.*, 3284 (1965).
(23) R. L. Carlin, *Transition Met. Chem.*, **1**, 1–31 (1965).
(24) J. DeO. Cabral, H. C. A. King, S. M. Nelson, T. M. Shepherd, and (in part) E. Körös, *J. Chem. Soc. A*, 1348 (1966).
(25) N. A. Daugherty and J. H. Swisher, *Inorg. Chem.*, **7**, 1651 (1968).
(26) D. Forster, K. Moedritzer, and J. R. VanWazer, *Inorg. Chem.*, **7**, 1138 (1968).
(27) A. Fratiello, R. E. Lee, D. P. Miller, and U. M. Nishrda, *Mol. Phys.*, **13**, 349 (1967).

Contribution from the School of Chemical Sciences, University of Illinois, Urbana, Illinois 61801

# Magnetic Exchange Interactions in Transition Metal Dimers. IV. High-Spin Cobalt(II)-2,2',2''-Triaminotriethylamine Complexes with Oxalate Inner-Sphere and Cyanate, Thiocyanate, Chloride, and Azide Outer-Sphere Bridges

D. MICHAEL DUGGAN[1] and DAVID N. HENDRICKSON*[2]

*Received October 24, 1974* AIC40741N

Infrared, electronic absorption, electron paramagnetic resonance (X and Q band), and variable-temperature magnetic susceptibility data are presented for the high-spin Co(II) complexes of the composition $[Co_2(tren)_2X_2](BPh_4)_2$, where $X^-$ = $OCN^-$, $SCN^-$, $Cl^-$, $N_3^-$, and $Ox^{2-}/2$ (Ox = oxalate), and tren is 2,2',2''-triaminotriethylamine. Infrared and electronic measurements show that in the oxalate case the cobalt ions are octahedrally coordinated by virtue of a bis-bidentate oxalate bridge. In the other cases the cobalt ions are (five-coordinate) trigonal-bipyramidally coordinated, and apparently each cobalt trigonal bipyramid is outer-sphere associated, probably via hydrogen bonding, with a second five-coordinate cobalt complex. Analysis of the electronic spectra of the five-coordinate complexes gives *Ds* and *Dt* values which are used in the analysis of the susceptibility. The susceptibility data (maximum in $\chi$ at $\sim$10°K) for the oxalate compound are least-squares fit to spin-only (i.e., $-2J\hat{S}_1\cdot\hat{S}_2$) equations to give $J = -3.1$ cm$^{-1}$ and $g = 2.21$. Indications of very weak ($|J| < 0.5$ cm$^{-1}$) antiferromagnetic interactions ($N_3^- > OCN^- > Cl^- \simeq NCS^-$) are found in the susceptibility curves for the other compounds through fitting to two different theoretical models, one for a monomeric $D_{3h}$-symmetry high-spin cobalt(II) complex and the other for a cobalt(II) dimer including single-ion zero-field splitting and isotropic exchange interaction. The dimeric nature of these complexes is further substantiated by the complexity (easily nine maxima in the 0–10-kG range for a spectrum showing *no* hyperfine) of the $\sim$12°K X-band EPR spectra of powdered samples. A qualitative discussion of the many features and temperature dependence of the $\sim$90 and 4.2°K Q-band (0–15-kG range) spectra for the complexes is presented. An interesting power saturation effect is noted.

## Introduction

In view of the large number and detailed character of the chemical, magnetic, and spectroscopic studies that have been carried out on divalent copper and nickel coordination compounds, it is surprising that few such in-depth attacks have been launched on cobalt(II) complexes. In the past few years, the discovery that certain *low-spin* cobalt(II) complexes will bind molecular oxygen has led to detailed crystallographic[3] and spectroscopic[4] studies of these systems. In contrast *high-spin* cobalt(II) complexes have not been as thoroughly studied except perhaps in the area of electronic absorption spectroscopy[5] where the optical characteristics of Co(II) in various environments have been set out. Even though magnetic susceptibility and EPR are potentially of greater sensitivity with respect to electronic structure, they have been all but overlooked for high-spin cobalt(II) systems probably because of the very low temperatures that are required. Very recently Ball and Blake[6] have reported the variable-temperature (80–400°K) magnetic susceptibilities of a series of high-spin octahedral Co(II) dimers. They found, in comparison to the analogous nickel(II) complexes,[7] a decreased exchange interaction in the cobalt complexes and concluded that the $t_{2g}$ spin of $Co^{2+}$ probably makes a ferromagnetic contribution to the exchange interaction. As pointed out by Ball and Blake, any analysis of the magnetism of exchange-interacting Co(II) dimers needs to take into account spin–orbit coupling such as can be seen in the treatment by Lines.[8]

In this paper the results of a variable-temperature magnetic susceptibility and EPR study of the series $[Co_2(tren)_2X_2](BPh_4)_2$, where $X^-$ = $N_3^-$, $OCN^-$, $SCN^-$, $Cl^-$, and $Ox^{2-}/2$ and tren is 2,2',2''-triaminotriethylamine, are reported. The complexes will be shown to be dimeric, inner-sphere bridged in the oxalate (Ox) case and (most probably) outer-sphere bridged in the cases of the other X groups. Outer-sphere bridging where metal ions are associated via two hydrogen-bonding contacts of the type Cu–X···HN–Cu has been found[9–12] to propagate an exchange interaction in the series $[Cu_2(tren)_2X_2](BPh_4)_2$ with $X^-$ = $Br^-$, $Cl^-$, $OCN^-$, $SCN^-$, and $CN^-$. One point which adds to the worth of the material to be presented is that spectroscopic and crystallographic studies of $Co^{II}$–tren compounds are in the first case infrequent and of low level and in the second case nonexistent. Magnetic susceptibility data at room temperature for Co(tren)$(NCS)_2$ and Co(tren)$I_2$ were reported[13] in 1958 and a solution moment for aqueous $Co(tren)^{2+}$ was available[14] in 1963, all of which indicated the metal ion to be high spin with a moment near 4.7 BM. The electronic spectrum of aqueous $Co(tren)^{2+}$ was also reported[14] and it was shown to contrast with that for the $Co(dien)_2^{2+}$ octahedral system (dien is diethylenetriamine). At the time, however, no conclusive evidence for the structure of these tren molecules was presented. At most it could be concluded that the coordination number was probably 5. Very recent work[15] with the five-coordinate high-spin Co(II) complexes of hexamethylated tren, i.e., $Co(Me_6tren)X^+$, has provided spectral characteristics that will be of use in the present study. The X-ray structure has been reported for trigonal-bipyramidal $[Co(Me_6tren)Br]Br$.[16]

## Experimental Section

**Compound Preparation.** All of the manipulations in the preparation of a $[Co_2(tren)_2X_2](BPh_4)_2$ compound were carried out in the following manner using a Schlenk-type apparatus as shown in Figure 1. Single-necked flasks are charged with the following solutions: $\sim$1.5 ml of tren dissolved in $\sim$50 ml of water; 0.01 mol of the sodium salt of the bridging anion (e.g., $N_3^-$, $Cl^-$, $CN^-$, $OCN^-$, $SCN^-$, or

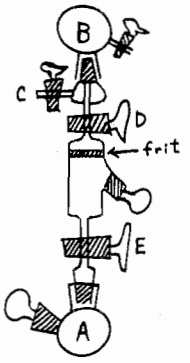


Figure 1. Schlenk-type apparatus.

$Ox^{2-}/2$) dissolved in 50 ml of $H_2O$; ~0.5 g of $NaBPh_4$ dissolved in 50 ml of $H_2O$; and distilled $H_2O$. All flasks are stoppered with serum stoppers and nitrogen gas is bubbled through each by a syringe needle. In flask A is placed ~0.01 mol of $Co(NO_3)_2 \cdot 6H_2O$ in ~75 ml of water, and then a serum stopper is fitted and nitrogen gas is flushed through the solution. All air in the reaction apparatus may be removed by application of vacuum to the side arm of flask B and then admitting nitrogen through A in alternating cycles. Each solution should be bubbled well for at least 2 hr before use. After this time, the tren solution is pumped through a syringe tube (polyethylene tubing with 18-gauge syringe needles inserted in each end) under pressure from its flask into flask A where it reacts with the cobalt ion. Depending on the amount of oxygen present, the solution is, at this point, light gray-green (small amount of $O_2$, satisfactory for most reactions except for $CN^-$) or light red-orange (no oxygen present). Exposure of any solution directly to air results in the formation of a brown material in the solution.

After the tren and $Co^{2+}$ solutions have been mixed, the bridging anion solution is added, also by pumping through a syringe tube. There may be a slight color change. While next pumping in the tetraphenylborate solution, the reaction flask is swirled rapidly and the precipitated product forms. The product is filtered by inverting the apparatus and applying vacuum to connection C. After all filtrate has been removed, distilled water is pumped into flask A and then used to wash the product. When the water has been drawn off, stopcocks D and E are both closed, flasks A and B are disconnected from the tube containing the precipitate, and by means of an adapter the tube is mounted on a vacuum line to be dried at $10^{-5}$ mm.

The colors of the samples prepared with the different anions are as follows: $N_3^-$, blue; $SCN^-$, blue; $OCN^-$, blue-green; $CN^-$, light blue; $Cl^-$, blue; $Ox^{2-}$, pink. The pink oxalate product is precipitated from a blue-green solution. The only one of the six compounds prepared that has extreme air-sensitivity is the cyanide. In the case of the cyanide compound, nitrogen gas from standard gas cylinders is inadequate, and while good product can be isolated by bubbling the $N_2$ gas through a series of two Cr(II)-scrubbing columns before use, this atmosphere was not found to be suitable for storage of the solid product for more than 0.5 hr. Because of this air sensitivity, the cyanide compound was not characterized.

Solid samples of all compounds other than the cyanide are relatively air stable (days of direct exposure to air discolor small particles of only the cyanate and thiocyanate materials). This air stability allowed accurate analytical work in the University of Illinois microanalytical laboratory, and Table I[17] shows that, with the exception of the cyanide which was not analyzed, very good analyses of C, H, N, and Co were obtained for all compounds.

An unsuccessful attempt to recrystallize one of these cobalt compounds was tried on a vacuum line. A sample of $[Co_2(tren)_2(N_3)_2](BPh_4)_2$ was placed in a 50-ml flask which was evacuated with a Hg-diffusion pump on a glass–grease vacuum line. A second flask containing acetonitrile was attached to another part of the line and was degassed five times by freeze–thaw cycles and then distilled into an adjacent flask where it was frozen to 77°K while the whole line was diffusion pumped. When the lowest pressure had been reached, the flask containing the cobalt compound was cooled and into it was condensed the warmed acetonitrile. Upon thawing of the acetonitrile, most of the cobalt material was dissolved and the solvent was slowly stripped off by condensing into a flask cooled by solid $CO_2$. Over the several-hour period required to do this a yellow coloration was noticed in the flask, indicating decomposition and no crystals were obtained.

A sample of **[Co(Me6tren)Cl]Cl** was prepared by the method of Ciampolini and Nardi.[18] Good C, H, N, and Co analyses were obtained (see Table I[17]).

Samples of $[Zn_2(tren)_2X_2](BPh_4)_2$ with $X^- = Ox^{2-}/2$, $N_3^-$, $NCS^-$, and $NCO^-$ were prepared for use as dopants in EPR studies and for ir spectral comparisons with the cobalt complexes. The zinc compounds were prepared in a fashion analogous to that used for the cobalt systems except, of course, inert-atmosphere conditions were unnecessary.

**Physical Measurements.** Normal 250–4000-$cm^{-1}$ ir spectra were run on a Perkin-Elmer Model 457 spectrophotometer while far-ir data were collected on a Beckman IR-11. It was found that KBr pellets of these cobalt compounds discolor and as such the ir samples were prepared as Nujol mulls in a drybox with a nitrogen atmosphere. Infrared spectra were run of these mulls between KBr plates and then electronic absorption spectra (Cary Model 14) were run of the same mull assemblies. Far-ir samples were prepared as mulls between polyethylene plates. For the electronic spectra in the visible region a reference mull was made of $NaBPh_4$ to balance the dispersion by the sample at lower wavelengths.

Magnetic susceptibility measurements were carried out as indicated in a previous paper.[10]

A variety of EPR instrumentation was required in order to obtain a full complement of data on these systems. The spectra are generally very temperature dependent in the 4–80°K region and are quite complicated at the higher temperatures when observed with X-band (~9-GHz) frequencies. Therefore, when X-band measurements were made, an Air Products Heli-tran liquid helium cooling system was employed in order to cool the sample. The lowest sample temperature obtainable with our setup is 12–15°K as gauged by an iron-doped gold thermocouple. The spectrometer used for the X-band studies is the Varian E-9 console and E-101 microwave bridge in conjunction with a 6-in., 10-kG magnet.

Q-Band measurements (~35 GHz) were also carried out; the apparatus used consisted of a Varian V-4561 microwave bridge and a 6-in. magnet equipped with tapered-pole pieces to extend the highest field to 15.5 kG. The field was controlled with a Hall-effect probe and a Varian Fieldial assembly. Because there was no frequency counter available to monitor the microwave output and the Fieldial sweep ranges are only roughly calibrated, the $g$ values on this apparatus could be determined to no better than ±0.05 at $g = 2.00$, which is however adequate considering the broad range over which signals are observed and their inherent line widths.

All Q-band spectra were run at either of two temperatures, 90 or 4.2°K. These temperatures were obtained by having the wave guide and sample cavity suspended into a glass double-dewar assembly which is necked at the bottom to fit the magnet gap. For the higher of the two temperatures the vacuum jacket separating the inner reservoir (wherein resides the waveguide) from the liquid nitrogen jacket was allowed a 100–200 Torr partial pressure of $N_2$ gas and the outside reservoir was filled with liquid nitrogen; thus, a thermal leak was established so that the inner reservoir and sample is cooled close to liquid nitrogen temperature (~90°K by measurement with an Fe-doped Au thermocouple). For the low-temperature limit the inner reservoir is charged with liquid helium so that the cavity is completely immersed in this refrigerant. No temperatures intermediate between the two indicated could be maintained sufficiently stable for recording spectra.

## Theory and Calculations

In this paper magnetic susceptibility data to 4.2°K are presented for three different types of high-spin cobalt(II) complexes: a trigonal-bipyramidal monomer [Co(Me6tren)Cl]Cl, weakly exchange-interacting outer-sphere-associated trigonal-bipyramidal dimers, and one bis-bidentate $\mu$-oxalato dimer, $[Co_2(tren)_2Ox](BPh_4)_2$. These high-spin Co(II) systems have single-ion zero-field interactions of several wave numbers, and when weak exchange interactions are present where the exchange parameter is less than ~2 $cm^{-1}$, exact diagonalization of the Hamiltonian matrices including zero-field, exchange, and Zeeman interactions as a function of magnetic field is desirable to fit the susceptibility data. In the following we will sketch some of the theoretical

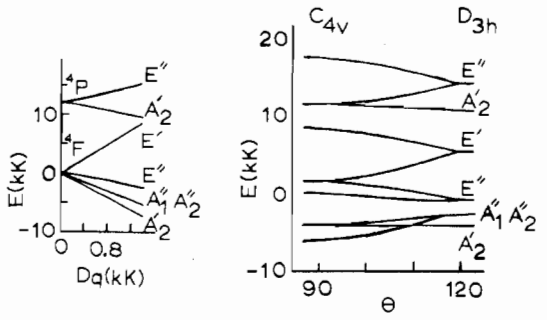


Figure 2.

models that we have used in conjunction with a simplex least-squares computer program to fit the data.

For a trigonal-bipyramidal complex with $D_{3h}$ symmetry the following ordering of one-electron orbitals would be expected: $d_{\pm1}$ ($d_{xz}$, $d_{yz}$) < $d_{\pm2}$ ($d_{xy}$, $d_{x^2-y^2}$) < $d_0$ ($d_{z^2}$). The relevant $d^7$ free-ion states are split as in the left side of Figure 2. For future reference the energy-state correlation diagram between $D_{3h}$ and $C_{4v}$ symmetries (square pyramidal, $\theta = 90°$) is also depicted in Figure 2, right side.[5] Wood[19,20] has parameterized the state splittings with the one-electron parameters $Ds$ and $Dt$ where

$$Ds = (1/14)(4Z_a/b^3 - 3Z_e/a^3)\langle r^2\rangle$$

$$Dt = (1/168)(16Z_a/b^5 - 9Z_e/a^5)\langle r^4\rangle$$

The $Z$'s are the effective ligand charges and $a$ and $b$ are metal–ligand distances for the equatorial and axial ligands, respectively. The one-electron matrix elements of the trigonal-bipyramidal crystal field operator $V_0$ are found to be $\langle 0|V_0|0\rangle = 2Ds + 6Dt$, $\langle \pm1|V_0|\pm1\rangle = Ds - 4Dt$, and $\langle \pm2|V_0|\pm2\rangle = -2Ds + Dt$. Writing out the determinantal wave functions for the ($d^7$) $^4F$ and $^4P$ term states (actually best carried out in hole formalism), the following crystal field energy matrix elements can be found

$$\langle {}^4E''(P)|V_0|{}^4E''(P)\rangle = (7/5)Ds + \Delta$$

$$\langle {}^4A_2'(P)|V_0|{}^4A_2'(P)\rangle = (-14/5)Ds + \Delta$$

$$\langle {}^4E'(F)|V_0|{}^4E'(F)\rangle = 7Dt$$

$$\langle {}^4E''(F)|V_0|{}^4E''(F)\rangle = (3/5)Ds - Dt$$

$$\langle {}^4A_2''(F)|V_0|{}^4A_2''(F)\rangle = \langle {}^4A_1''(F)|V_0|{}^4A_1''(F)\rangle = -Ds - 3Dt$$

$$\langle {}^4A_2'(F)|V_0|{}^4A_2'(F)\rangle = (4/5)Ds - 6Dt$$

Off-diagonal elements are present between the $^4A_2'$(P) and $^4A_2'$(F) states as well as between the two $^4E''$ states. In that we are only concerned with the $^4A_2'$(F) ground state, only one interaction is important

$$\langle {}^4A_2'(P)|V_0|{}^4A_2'(F)\rangle = 4Dt - (12/5)Ds$$

Spin–orbit interactions are introduced with the operator $H_{so} = k\lambda(\hat{L}_z\hat{S}_z + {}^1/_2\hat{L}_+\hat{S}_- + {}^1/_2\hat{L}_-\hat{S}_+)$, where $k$ the orbital reduction factor and $\lambda$ is the spin–orbit coupling constant. Since the $^4A_2'$ ground state has $M_L = 0$, there are no first-order spin–orbit terms; however, the following off-diagonal elements are found

$$\langle {}^4E''\ 3, 1, {}^3/_2, {}^1/_2|H_{so}|{}^4A_2'\ 3, 0, {}^3/_2, {}^3/_2\rangle = 3\lambda k$$

$$\langle {}^4E''\ 3, -1, {}^3/_2, -{}^1/_2|H_{so}|{}^4A_2'\ 3, 0, {}^3/_2, -{}^3/_2\rangle = 3\lambda k$$

$$\langle {}^4E''\ 3, 1, {}^3/_2, -{}^1/_2|H_{so}|{}^4A_2'\ 3, 0, {}^3/_2, {}^1/_2\rangle = 2\sqrt{3}\lambda k$$

$$\langle {}^4E''\ 3, -1, {}^3/_2, {}^3/_2|H_{so}|{}^4A_2'\ 3, 0, {}^3/_2, {}^1/_2\rangle = 3\lambda k$$

$$\langle {}^4E''\ 3, 1, {}^3/_2, -{}^3/_2|H_{so}|{}^4A_2'\ 3, 0, {}^3/_2, -{}^1/_2\rangle = 3\lambda k$$

$$\langle {}^4E''\ 3, -1, {}^3/_2, {}^1/_2|H_{so}|{}^4A_2'\ 3, 0, {}^3/_2, -{}^1/_2\rangle = 2\sqrt{3}\lambda k$$

At this point the eigenvalues and eigenfunctions under spin–orbit coupling and the crystal field operator were calculated using perturbation theory. The energy results are

$$E({}^4A_2'(F)\ \pm{}^3/_2) = (4/5)Ds - 6Dt + (4Dt - (12/5)Ds)^2/(-\Delta + (18/5)Ds - 6Dt) + 9\lambda^2k^2/(0.2Ds - 5Dt)$$

$$E({}^4A_2'(F)\ \pm{}^1/_2 = (4/5)Ds - 6Dt + (4Dt - (12/5)Ds)^2/(-\Delta + (18/5)Ds - 6Dt) + 21\lambda^2k^2/(0.2Ds - 5Dt)$$

and the energy splitting between these states is $12\lambda^2k^2/(0.2Ds - 5Dt)$ or $12\lambda^2k^2/({}^4A_2' - {}^4E'')$ which agrees with the results given by Wood.[19] It should be noted that the wave function labels used are no longer strictly correct, as $M_S$ is no longer a valid quantum number and double-group symmetries are needed. The above designations will be used however for clarity and continuity. The spin–orbit eigenfunctions are

$$|{}^4A_2'\ \pm{}^3/_2\rangle = |3, 0, {}^3/_2, \pm{}^3/_2\rangle + (4Dt - 2.4Ds)/(-\Delta + 3.6Ds - 6Dt)|1, 0, {}^3/_2, \pm{}^3/_2\rangle + 3\lambda k/(0.2Ds - 5Dt)|3, \pm1, {}^3/_2, \pm{}^1/_2\rangle$$

and

$$|{}^4A_2'\ \pm{}^1/_2\rangle = |3, 0, {}^3/_2, \pm{}^1/_2\rangle + (4Dt - 2.4Ds)/(-\Delta + 3.6Ds - 6Dt)|1, 0, {}^3/_2, \pm{}^1/_2\rangle + 2\sqrt{3}\lambda k/(0.2Ds - 5Dt)|3, \pm1, {}^3/_2, \mp{}^1/_2\rangle + 3\lambda k/(0.2Ds - 5Dt)|3, \mp1, {}^3/_2, \pm{}^3/_2\rangle$$

To calculate the magnetic field effect on the system the Zeeman operator

$$H_H = \beta(k\hat{L}_z + 2\hat{S}_z)H_z + \beta({}^1/_2k(\hat{L}_+ + \hat{L}_-) + (\hat{S}_+ + \hat{S}_-))H_x$$

is used, where axial symmetry is assumed. The diagonal Zeeman elements in the $^4A_2'$ 4 × 4 matrix are (where $G = (4Dt - 2.4Ds)/(-\Delta + 3.6Ds - 6Dt)$)

$$\langle {}^4A_2'\ \pm{}^3/_2|H_{H_z}|{}^4A_2'\ \pm{}^3/_2\rangle = \pm3\beta H_z + G^2(\pm3\beta H_z) + (3\lambda k/(0.2Ds - 5Dt))^2(\pm\beta H_z k \pm \beta H_z)$$

and

$$\langle {}^4A_2'\ \pm{}^1/_2|H_{H_z}|{}^4A_2'\ \pm{}^1/_2\rangle = \pm\beta H_z + G^2(\pm\beta H_z) + (2\sqrt{3}\lambda k/(0.2Ds - 5Dt))^2(\pm\beta k H_z \mp \beta H_z) + (3\lambda k/(0.2Ds - 5Dt))^2(\beta k H_z \pm 3\beta H_z)$$

Likewise the nonzero off-diagonal Zeeman elements are found to be

$$\langle {}^4A_2'\ \pm{}^1/_2|H_x|{}^4A_2'\ \pm\ {}^3/_2\rangle = \sqrt{3}\beta H_x + 6\sqrt{3}k^2\lambda\beta H_x/(0.2Ds - 5Dt) + 12\sqrt{3}\beta H_x\lambda^2k^2/(0.2Ds - 5Dt)^2 + G^2\sqrt{3}\beta H_x$$

and

$$\langle {}^4A_2'\ \mp\ {}^1/_2|H_x|{}^4A_2'\ \pm{}^1/_2\rangle = 2\beta H_x + 12\beta k^2\lambda H_x/(0.2Ds - 5Dt) + 36\beta k^2\lambda^2 H_x/(0.2Ds - 5Dt) + 2\beta H_x G^2$$

In order to calculate the energies and susceptibilities of the $^4A_2'$ states a matrix is set up with the $\pm{}^1/_2$ levels at zero energy at zero field and the $\pm{}^3/_2$ Kramers doublet at $-12\lambda^2k^2/(0.2Ds - 5Dt)$ which is higher in energy. The diagonal or off-diagonal Zeeman elements are added and due to the potentially comparable size of the zero-field splitting between the above $\pm{}^3/_2$ and $\pm{}^1/_2$ doublets relative to the Zeeman terms, the matrix is diagonalized numerically by a computer, once to determine the energies with the magnetic field $H$ in the $z$

direction and again to find them for $H_z = 0$ and $H_x = H_y \neq 0$. For each orientation the slope of $E$ vs. $H$ is determined for both of the Kramers doublets at the desired magnetic field; this slope is the magnetic moment for the $i$th energy level

$$\mu_i = -\partial E_i/\partial H$$

The magnetic susceptibility of the system is then calculated as a function of temperature using the van Vleck formula. The simplex least-squares program then compares calculated and observed susceptibility curves and changes the parameters (e.g., $Ds$, $Dt$, and $\lambda$) to get the best fit. The above theoretical monomer model will be referred to as model A. The above equations should be compared with those set out by Bertini and coworkers.[5,21]

Model B is an effective spin Hamiltonian theoretical model for an exchange-interacting high-spin Co(II) dimer including single-ion zero-field splitting. For two metal ions in a dimeric complex, each having three unpaired electrons and no orbital angular momentum in the ground state, the effective spin Hamiltonian may be written

$$\mathcal{H} = -2JS_1 \cdot S_2 - D(S_{1z}^2 + S_{2z}^2) - g_i\beta H_i \cdot S_i \quad i = x, y, z$$

Here the term in $J$ represents the isotropic exchange interaction, that in $D$ represents the single-ion zero-field splitting, and the third term is the Zeeman interaction ignoring orbital momentum (second-order effects of this sort will be absorbed into the TIP correction). In the Zeeman term the total dimer spin $S'$ is used. The coupled basis functions, $|S'MS'\rangle$, can be easily written with the Wigner coefficients as tabulated, for example, in a book by Condon and Shortley.[34] If one operates on the coupled wave functions with the above Hamiltonian exclusive of the Zeeman term, the following matrix elements are obtained

$$\langle 3 \pm 3|H_0|3 \pm 3\rangle = -12J - (9/2)D$$
$$\langle 3 \pm 2|H_0|3 \pm 2\rangle = -12J - (5/2)D$$
$$\langle 3 \pm 1|H_0|3 \pm 1\rangle = -12J - (13/10)D$$
$$\langle 30|H_0|30\rangle = -12J - (9/10)D$$
$$\langle 1 \pm 1|H_0|3 \pm 1\rangle = -(2/5)\sqrt{6}D$$
$$\langle 10|H_0|30\rangle = -(6/5)D$$
$$\langle 2 \pm 2|H_0|2 \pm 2\rangle = -6J - (5/2)D$$
$$\langle 2 \pm 1|H_0|2 \pm 1|\rangle = -6J - (5/2)D$$
$$\langle 20|H_0|20\rangle = -6J - (5/2)D$$
$$\langle 00|H_0|20\rangle = -2D$$
$$\langle 1 \pm 1|H_0|1 \pm 1\rangle = -2J - (17/10)D$$
$$\langle 10|H_0|10\rangle = -2J - (41/10)D$$
$$\langle 00|H_0|00\rangle = -(5/2)D$$

Because $D$ and $J$ could be on the same order of magnitude for our systems, the zero-field energy matrix $H_0$ is *not* solved by perturbation theory. Instead, the following Zeeman terms are added and the resulting matrices are diagonalized as a function of magnetic field. The required Zeeman elements with $i = z$ are

$$\langle 3 \pm 3|H_z'|3 \pm 3\rangle = \mp 3g_z\beta H_z$$
$$\langle 3 \pm 2|H_z'|3 \pm 2\rangle = \mp 2g_z\beta H_z$$
$$\langle 3 \pm 1|H_z'|3 \pm 1\rangle = \mp g_z\beta H_z$$
$$\langle 2 \pm 2|H_z'|2 \pm 2\rangle = \mp 2g_z\beta H_z$$
$$\langle 2 \pm 1|H_z'|2 \pm 1\rangle = \mp g_z\beta H_z$$
$$\langle 1 \pm 1|H_z'|1 \pm 1\rangle = \mp g_z\beta H_z$$

And those obtained with

$$H_x' = {}^1/_2 g_x\beta H_x(\hat{S}_+' + \hat{S}_-')$$

where the magnetic field is now in the $x$ direction are

$$\langle 3 \pm 2|H_x'|3 \pm 3\rangle = -g_x\beta H_x\sqrt{6}/2$$
$$\langle 3 \pm 1|H_x'|3 \pm 2\rangle = -g_x\beta H_x\sqrt{(5/2)}$$
$$\langle 30|H_x'|3 \pm 1\rangle = -g_x\beta H_x\sqrt{3}$$
$$\langle 2 \pm 1|H_x'|2 \pm 2\rangle = -g_x\beta H_x$$
$$\langle 20|H_x'|2 \pm 1\rangle = -g_x\beta H_x\sqrt{(3/2)}$$
$$\langle 10|H_x'|1 \pm 1\rangle = -g_x\beta H_x\sqrt{2}/2$$

Calculating the eigenvalues of the energy matrix with the field in the $x$ and $z$ direction (axial system), numerically differentiating with respect to field, and calculating the population-weighted average of moments will yield $\chi_\parallel$ and $\chi_\perp$ values for this system, as was done above for the trigonal-bipyramidal monomer.

Model C is an admittedly simple model wherein the temperature dependence of the magnetic susceptibility for a Co(II) dimer is assumed to be due entirely to exchange interaction with an assumed isotropic $g$ and intermolecular exchange interactions accounted for by a Weiss constant. As per one of the three models used by Ball and Blake,[7] the susceptibility of the pair of Co(II) ions is given as

$$\chi_M = \frac{2N\beta^2g^2}{kT}\left[\frac{e^{-10x} + 5e^{-6x} + 14}{e^{-12x} + 3e^{-10x} + 5e^{-6x} + 7}\right]$$

where $x = J/kT$.

In all cases values of

$$SE = \left\{\sum_{i=1}^{n}[\mu_{eff}(obsd)_i - \mu_{eff}(calcd)_i]^2/(n-K)\right\}^{1/2}$$

where $n$ is the number of observables and $K$ is the number of parameters, are given as a measure of the discrepancy between the experimental and calculated curves. It is unfortunate that we are not able to calculate a correlation matrix for the various parameters used in the different fittings.

## Results and Discussion

It is our contention, based firmly on spectroscopic evidence, that the $[Co_2(tren)_2Ox](BPh_4)_2$ compound is an $\mu$-oxalato-bridged dimer with a bis-bidentate inner-sphere bridge and that the other $[Co_2(tren)_2X_2](BPh_4)_2$ ($X^- = OCN^-$, $SCN^-$, $N_3^-$, and $Cl^-$) compounds have, on the contrary, five-coordinate trigonal-bipyramidal cobalt(II) cations that are pairwise associated in some outer-sphere-bridged fashion. It is very relevant to point out that we have at present established, via X-ray crystal structures, the presence of such an outer-sphere association in four Cu(II) compounds[9-12] (e.g., $[Cu_2(tren)_2X_2](BPh_4)_2$ where $X^- = CN^-$, $OCN^-$, $SCN^-$, and $Cl^-$) and one high-spin Mn(II) compound, $[Mn_2(tren)_2(NCS)_2](BPh_4)_2$.[22] In the two following sections infrared and electronic data bearing on the local Co(II) environment will be summarized. In the susceptibility and EPR sections the consequences of the inner- or outer-sphere associations will be delineated and the results of attempts to quantize the exchange parameters for these Co(II) dimers will be discussed.

**Infrared Spectra.** Figure 3 illustrates the Nujol mull ir spectra of $[Co_2(tren)_2X_2](BPh_4)_2$ compounds where $X^- = N_3^-$ (A), $OCN^-$ (B), and $SCN^-$ (C). The frequencies of relevant bands are given in Table II.[17] For example, the asymmetric azide stretch, $\nu_{as}(N_3^-)$, seen in tracing A appears at 2100 $cm^{-1}$, whereas, for tracings B and C the corresponding bands are $\nu_{as}(OCN^-)$ 2220 $cm^{-1}$ and $\nu_{as}(SCN^-)$ 2090 $cm^{-1}$, respectively. Comparison of the $N_3^-$ and $SCN^-$ spectra shows that the symmetric azide stretch has negligible intensity. On the other

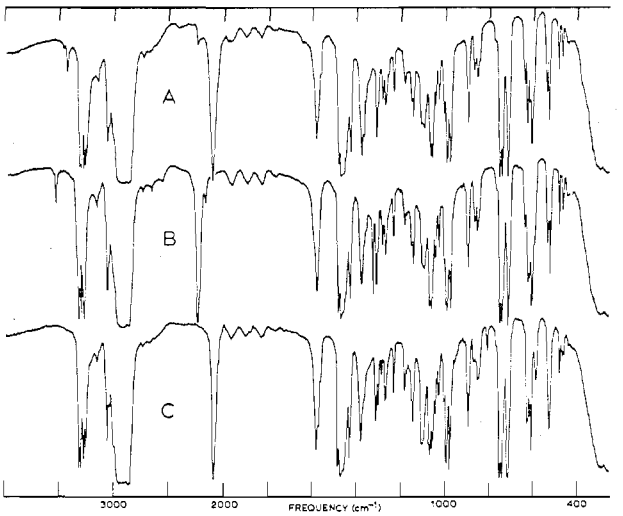


Figure 3. Nujol mull ir spectra of $[Co_2(tren)_2X_2](BPh_4)_2$ where $X^- = N_3^-$ (A), $OCN^-$ (B), and $SCN^-$ (C).

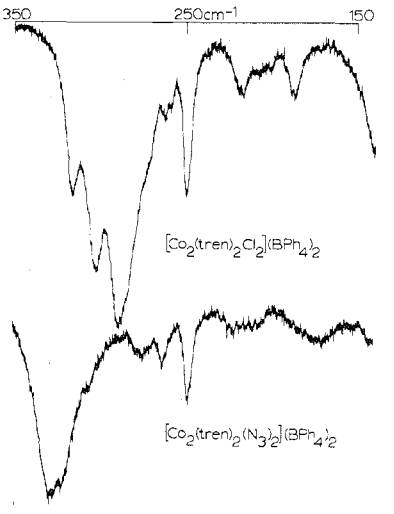


Figure 4. Far-ir spectra of Nujol mulls of $[Co_2(tren)_2X_2](BPh_4)_2$ where $X^- = Cl^-$ (top) and $X^- = N_3^-$ (bottom).

hand, a $\nu_s(OCN^-)$ band is seen at 1329 $cm^{-1}$ with medium intensity.

It has been our experience from X-ray structures and ir characteristics of analogous "outer-sphere" Cu(II) and Mn(II) and inner-sphere Ni(II) tren dimers[10,22-25] that the pattern of H–N–H bending vibrations (determined to be such by deuteration) in the region 1200–1400 $cm^{-1}$ is very indicative of the structural characteristics of the complex. For the octahedral nickel complexes, the local symmetry of the tren group is lower than that found for the trigonal-bipyramidal copper and manganese complexes. As a consequence the nickel 1200–1400-$cm^{-1}$ pattern is distinctly different from and more complicated than either the copper or the manganese pattern, both of which show a reasonable similarity. In short, careful scrutiny and comparison of the cobalt 1200–1400-$cm^{-1}$ pattern with patterns for structurally characterized Cu(II), Ni(II), and Mn(II) compounds conclusively point to the presence of trigonal-bipyramidal cobalt(II) cations in the azide, cyanate, thiocyanate, and chloride compounds. Thus, the cobalt, copper, and manganese patterns show strong resemblances. The small differences in patterns probably point to different degrees of distortions in the trigonal bipyramids. Perhaps another indicator of a different distortion in the cobalt systems is the dramatically enhanced intensity of the ~1100-$cm^{-1}$ band in the cobalt spectra.

As with the other metal–tren oxalates, the cobalt oxalate compound does not have appreciable intensity in this ~1100 $cm^{-1}$ band. Support for proposing octahedral cobalt with a bis-bidentate oxalate is drawn from the sharp unsplit appearance of the three observed oxalate bands [1640 $cm^{-1}$ (vs), 789 $cm^{-1}$ (m), and 579 $cm^{-1}$ (mw)].

Additional supporting evidence for five-coordinate trigonal-bipyramidal cobalt in $[Co_2(tren)_2Cl_2](BPh_4)_2$ can be seen in the position of the Co–Cl stretch. Nakamoto et al.[26] have shown that the terminal Co–Cl stretching vibrations occur in the range 306–347 $cm^{-1}$, which is more than 150 $cm^{-1}$ higher in energy than the range expected (155–186 $cm^{-1}$) for bridging Co–Cl–Co situations. Figure 4 shows a comparison between the ir spectra of the cobalt azide and cobalt chloride compounds in the region from 150 to 350 $cm^{-1}$. The spectra are seen to be basically the same with the exceptions of a strong band for the azide at 328 $cm^{-1}$ and a strong band in the chloride at 288 $cm^{-1}$. This latter band is assigned as the Co–Cl band and its location indicates that the Co–Cl band is basically terminal in nature and thus the cobalt ions are five-coordinate. The fact that the Co–Cl band is somewhat lower than the above range can be interpreted as a result of an Co–Cl···HN–Co hydrogen-bond interaction as was found for $[Cu_2(tren)_2Cl_2](BPh_4)_2$.[12]

As a final note in this section it should be mentioned that we have found a point for point coincidence, including the ~1100-$cm^{-1}$ bands, of the cobalt ir spectra with those for the $[Zn_2(tren)_2X_2](BPh_4)_2$ compounds where $X^- = OCN^-$, $SCN^-$, $N_3^-$, and $Ox^{2-}/2$. The details of the splittings around 1300 $cm^{-1}$ mark the remarkably similar structures for the cobalt and zinc analogs.

**Electronic Spectra.** In addition to substantiating the above proposals as to local cobalt environments, an analysis of the electronic spectra of the $[Co_2(tren)_2X_2](BPh_4)_2$ compounds provides many parameters that will assist in the explanation of the magnetic data.

Many efforts have been made at interpretating spectra of $D_{3h}$-symmetry $d^7$ compounds, such as that by Venanzi and coworkers[27] where they were mostly concerned with low-spin complexes and crystal field treatments of high-spin Co(II) by Ciampolini[28] and Wood.[19] Ciampolini reported energy level diagrams for both trigonal-bipyramidal and square-pyramidal Co(II) and correlations between them.

The $D_{3h}$ energy level diagram is sketched in Figure 2. Five ligand field transitions from the $^4A_2'$ ground state are expected. One of these (accidental degeneracy), $^4A_2' \rightarrow [^4A_2'', {}^4A_1'']$, will be of very low energy and difficult to observe, whereas, $^4A_2' \rightarrow {}^4E''$, $^4E'$, $^4A_2'(P)$, and $^4E''(P)$ transitions all might be detectable. Energy expressions have been given above for $D_{3h}$ symmetry and the spectral features for the Co–tren complexes of azide, cyanate, thiocyanate, chloride, and oxalate are given in Table III. Reproductions of the spectra of the azide, cyanate, and thiocyanate are given in Figure 5. Keying on the fact that, as can be seen in the $D_{3h}$ energy diagram, the $^4A_2'(F) \rightarrow {}^4A_2'(P)$ transition energy is relatively invariant of crystal field strength, assignments for the various bands of the azide, cyanate, thiocyanate, and chloride compounds have been made assuming the symmetry about the cobalt center to be close to $D_{3h}$. The assignments, resulting $Ds$, $Dt$, and $\Delta$ parameters, and calculated band positions are given in Table III. The $^4F$–$^4P$ separation for the free ion is 14.56 kK so that it can be seen that reasonable values of the orbital reduction are found. It is unfortunate that the $^4E'(F)$ and $(^4A_2'', {}^4A_1'')$ bands cannot be identified.

The crystal field strengths required by the $D_{3h}$ equations for the assignments in Table III are somewhat greater than seems reasonable, and it is possible that strict $D_{3h}$ symmetry does not really apply here. An alternative assignment, or perhaps more refined one, may be based upon the correlation

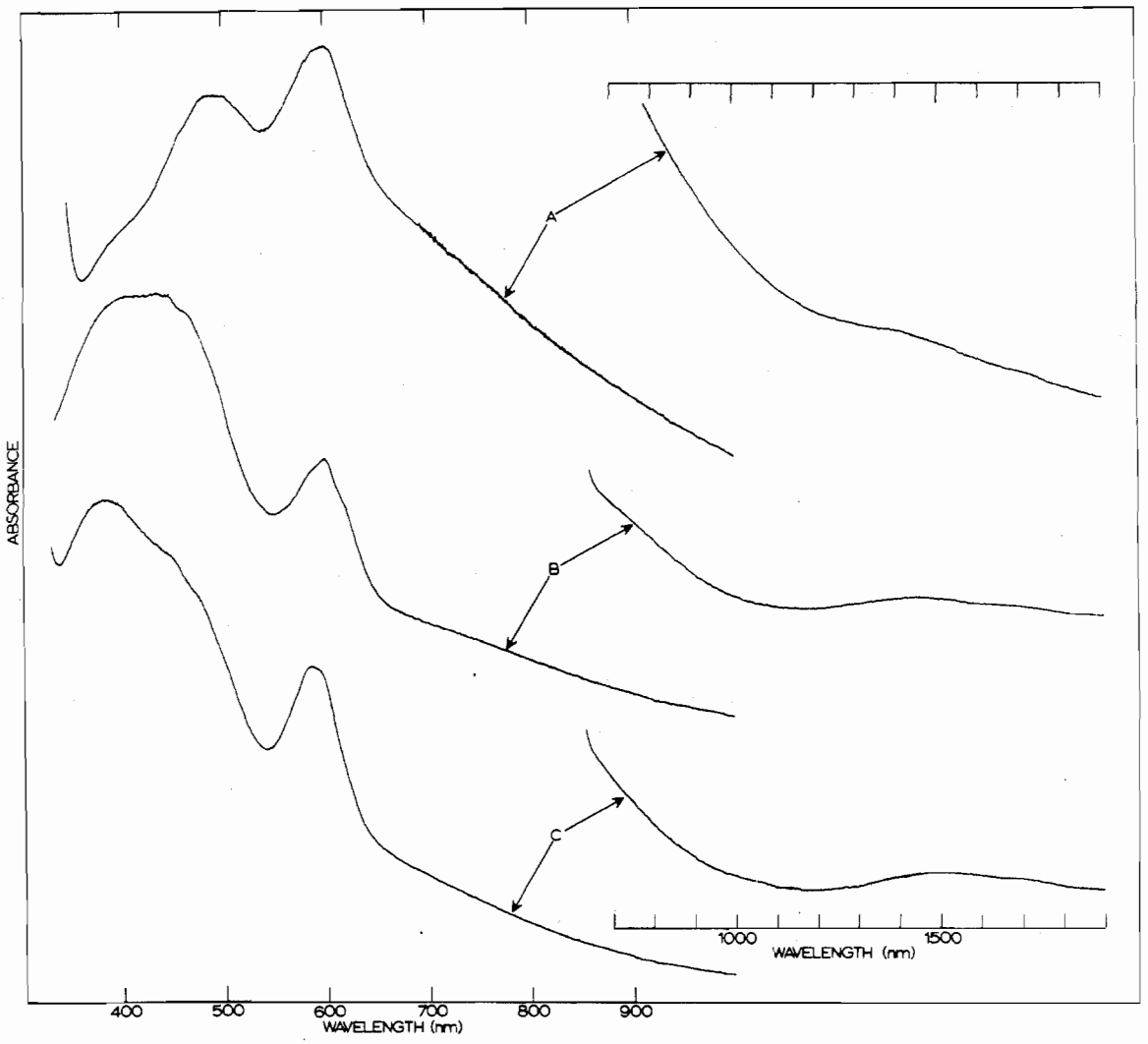


Figure 5. Electronic absorption spectra for room-temperature Nujol mulls of $[Co_2(tren)_2X_2](BPh_4)_2$ where $X^- = N_3^-$ (A), $OCN^-$ (B), and $SCN^-$ (C).

diagram between $D_{3h}$ and $C_{4v}$ (square pyramidal) symmetry given by Ciampolini.[28] Several observations may be made if the angle between two of the equatorial ligand sites is taken as 110°. For the same choice of parameters the $^4A_2'$–$^4E''$ separation becomes larger and the $^4E''$ level splits. It could be that the high frequency (7000 $cm^{-1}$) observed for the $^4A_2' \rightarrow {}^4E''$ transition in these tren compounds compared to that observed for the Me6tren systems (5800 $cm^{-1}$) is a result of this distortion. Also, there is observed at ~1700 nm (see Figure 5) a weak band which may be the lower split component of the $^4E''$ transition. The relative constancy in the $^4A_2'$-(F)–$^4A_2'$(P) energy with the trigonal angle is noted and is consistent with observation, and the splitting of the $^4E''$(P) state cannot be ruled out due to the complexity of this region of the spectrum. If the molecule is distorted, this more refined interpretation should be followed. While it is difficult to reevaluate *Ds* from the highest bands, the best estimate of the "distorted" $D_{3h}$-symmetry $^4A_2' \rightarrow {}^4E''$ band might be taken as closer to the lower energy of the two observed near-ir bands, i.e., say ~1650 nm (6000 $cm^{-1}$). In this case $Dt \simeq 1240$ $cm^{-1}$, $\Delta \simeq 12{,}800$ $cm^{-1}$ (a 12% reduction from free ion), and the $^4A_2' \rightarrow {}^4E''$ band is predicted to lie at ~15,000 $cm^{-1}$, which is more reasonable than that obtained previously. In any event it may be said that the observed spectral features are consistent with a distorted trigonal-bipyramidal stereochemistry and that at least reasonable estimates of *Ds*, *Dt*, and $\Delta$ can be made for use in predicting the magnetic properties of these systems.

As compared with the spectra of the distorted trigonal-bipyramidal Co–tren complexes, the spectrum of $[Co_2(tren)_2Ox](BPh_4)_2$, reproduced in Figure 6 and enumerated in Table III, shows marked dissimilarity. The $^4F$ state in $O_h$ symmetry splits into a $^4T_{1g}$ ground state and $^4T_{2g}$ and $^4A_{2g}$ excited states. The $^4P$ term does not split in perfect $O_h$ symmetry but transforms as $^4T_{1g}$. The complexity of the 20,000-$cm^{-1}$ region for the oxalate compound is undoubtedly due to the distortion in octahedral symmetry for this system and the resultant splitting of both the triply degenerate ground and excited states. All observed strong and weak features of

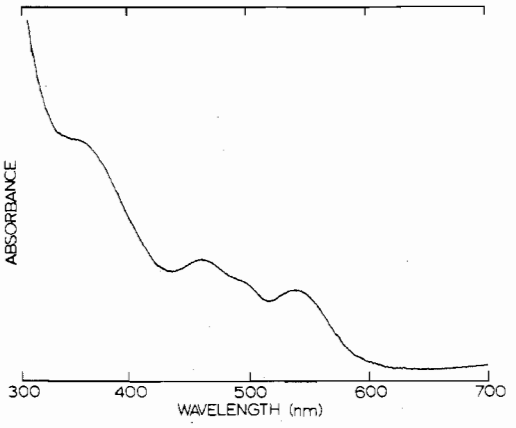


Figure 6. Electronic absorption spectrum of a room-temperature Nujol mull of $[Co_2(tren)_2Ox](BPh_4)_2$.

Table III. Electronic Spectral Data for $[Co_2(tren)_2X_2](BPh_4)_2$[a]

| X⁻ | Band position, A | Band position, kK | Assignment | Ligand field parameters |
|---|---|---|---|---|
| $C_2O_4^{2-}/2$ | 3,700 vs, sh | 27.0 | | |
| | 4,680 s | 21.4 | | |
| | 4,970 w, sh | 20.1 | | |
| | 5,410 m | 18.5 | | |
| | 6,900 vw, sh | 14.5 | | |
| | 9,900 vw, br | 10.1 | | |
| | 12,000 vw | 8.33 | | |
| $NCS^-$ | 3,850 s | 26.0 | | $Ds = 857\ cm^{-1}$ |
| | 4,530 w, sh | 22.1 | | $Dt = 1414\ cm^{-1}$ |
| | 4,830 vw, sh | 20.7 | $^4E''(P) \leftarrow {}^4A_2'(F)$ | $\Delta = 11{,}700\ cm^{-1}$ |
| | 5,860 m, sp | | $^4A_2'(P) \leftarrow {}^4A_2'(F)$ | |
| | 14,500 vw, br | | $^4E''(F) \leftarrow {}^4A_2'(F)$ | |
| $NCO^-$ | 4,050[b] | 24.7 | | $Ds = 1095\ cm^{-1}$ |
| | 4,400[b] | 22.7 | | $Dt = 1442\ cm^{-1}$ |
| | 4,690[b] | 21.3 | $^4E''(P) \leftarrow {}^4A_2'(F)$ | $\Delta = 11{,}990\ cm^{-1}$ |
| | 5,820 w, sh | 17.2 | | |
| | 5,990 m | 16.7 | $^4A_2'(P) \leftarrow {}^4A_2'(F)$ | |
| | 6,250 w, sh | 16.0 | | |
| | 7,600 vw, sh | 13.2 | | |
| | 14,300 vw, br | 6.99 | $^4E''(F) \leftarrow {}^4A_2'(F)$ | |
| $N_3^-$ | 4,940 | | | $Ds = 1024\ cm^{-1}$ |
| | 5,950 | | | $Dt = 1449\ cm^{-1}$ |
| | 7,420 | 13.5 | | $\Delta = 11{,}492\ cm^{-1}$ |
| | 14,200 | 7.04 | $^4E''(F) \leftarrow {}^4A_2'(F)$ | |
| | 4,570 m, sh | 21.9 | | |
| | 4,810 s | 20.8 | $^4E''(P) \leftarrow {}^4A_2'(F)$ | |
| | 5,110 m, sh | 19.6 | | |
| | 5,780 m, sh [c] | 17.3 [c] | | |
| | 6,050 s | 16.5 | $^4A_2'(P) \leftarrow {}^4A_2'(F)$ | |
| | 6,340 mw, sh | 15.8 | | |

[a] Nujol mull spectra at room temperature. [b] These three peaks are not well resolved. [c] KBr disk spectrum.

the spectrum may be fit to the energy level diagram including spin–orbit coupling given by Liehr[29] for the $d^7$ ion in an octahedral field. The best value of $Dq$ is close to 1000 $cm^{-1}$.

**Magnetic Susceptibility.** As stated earlier, the complicated single-ion magnetic properties of Co(II) require that careful study be undertaken to establish the presence of exchange coupling in these systems. For trigonal-bipyramidal high-spin cobalt(II), zero-field splitting of the $^4A_2'$ ground state into $\pm 3/2$ and $\pm 1/2$ Kramers doublets results in a decrease in the magnetic moment at low temperatures. This is due to the increased population of the $\pm 1/2$ doublet relative to the $\pm 3/2$ doublet. The onset of this decrease may appear to be due to an antiferromagnetic exchange effect, and to distinguish these two phenomena one must investigate quantitatively the functionality of the curvature in an $\mu_{eff}$ vs. $T$ plot, as well as the magnitude of decrease in $\mu_{eff}$. The experimentally observed data may be compared either with values expected for a monomeric Co(II) molecule or with those expected for a model cobalt(II) dimer.

The electronic spectrum of $[Co(Me_6tren)Cl]Cl$,[18] which is known to be monomeric, gives the parameters $Ds = 1047\ cm^{-1}$ and $Dt = 1444\ cm^{-1}$ ($k = 0.90$ and $\lambda$, the spin–orbit coupling for free-ion Co(II), is $-178\ cm^{-1}$). This gives a zero-field splitting ($D$) between the $\pm 1/2$ and $\pm 3/2$ Kramers doublets of 52.8 $cm^{-1}$. As described in the Theory and Calculations section, model A is to be used in the fitting of susceptibility data for a $D_{3h}$ symmetry monomer. Before we launch into a fitting of the data for $[Co(Me_6tren)Cl]Cl$, it is instructional to investigate the characteristics of the $\mu_{eff}$ vs. temperature curve using model A and certain selected parameters.

Figure 7 shows four $\mu_{eff}$ vs. temperature curves calculated with model A equations and different parameters. For curve C, where $Ds = 1047\ cm^{-1}$, $Dt = 1444\ cm^{-1}$, and $k = 1.0$ (determines magnitude of spin–orbit interaction and $\Delta$, the energy difference between the unsplit $^4F$ and $^4P$ states), it is found that at temperatures below 100°K the value of $\mu_{eff}$ decreases rapidly with a lower limit of ~3.6 BM at 5°K. This decrease arises from ~50-$cm^{-1}$ splitting of the ground state. As $Dt$ is increased, the $^4E''$ excited state separates further in energy from the $^4A_2'$ ground state, thus decreasing $D$, since the zero-field splitting is due, in part, to the second-order spin–orbit mixing of the $^4A_2'$ and $^4E''$ states. The increased $Dt$ effect is illustrated with curve B, where the decreased $D$ makes the attenuation of $\mu_{eff}$ noticeable only at lower temperatures. The parameters used in calculating curve A, most

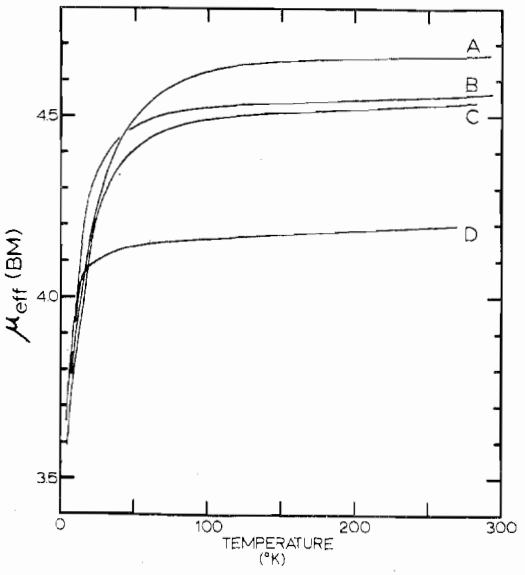


**Figure 7.** Theoretical effective magnetic moment curves for a monomeric high-spin Co(II) $D_{3h}$ system. The parameters used were as follows: A, $k = 1.0$, $Ds = 1047\ cm^{-1}$, $Dt = 1000\ cm^{-1}$; B, $k = 1.0$, $Ds = 1047\ cm^{-1}$, $Dt = 2000\ cm^{-1}$; C, $k = 1.0$, $Ds = 1047\ cm^{-1}$, $Dt = 1440\ cm^{-1}$; D, $k = 0.5$, $Ds = 1047\ cm^{-1}$, $Dt = 1440\ cm^{-1}$.

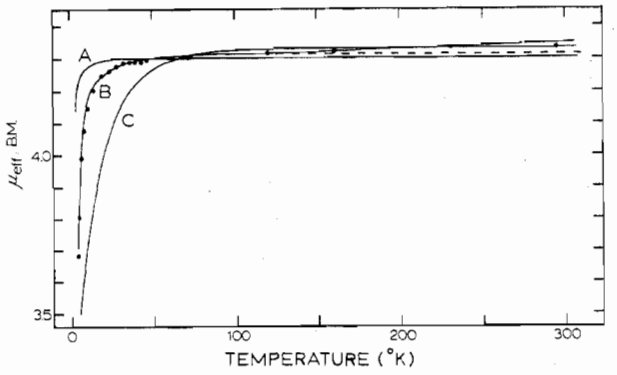


**Figure 8.** Least-squares fitting of the magnetic susceptibility data for [Co(Me$_6$tren)Cl]Cl to model A for a $D_{3h}$-symmetry monomer. The following conditions were imposed on the fit: A, no spin–orbit coupling, $^4A_2'(F)$–$^4A_2'(P)$ mixing only, and final parameters are $k = 0$, $Ds = 1000$ cm$^{-1}$, and $Dt = 2540$ cm$^{-1}$ (TIP = 0); B, spin–orbit coupling and $^4A_2'(F)$–$^4A_2'(P)$ mixing allowed and final parameters are $k = 0.53$, $Ds = 8885$ cm$^{-1}$, and $Dt = 2078$ cm$^{-1}$ (TIP = 0.00020); C, spin–orbit coupling only and final parameters are $k = 0.98$, $Ds = 114$ cm$^{-1}$, and $Dt = 1360$ cm$^{-1}$ (TIP = 0).

importantly $Dt = 1000$ cm$^{-1}$, lead to a very large $D$ and thus an appreciably larger decrease in $\mu_{eff}$. Finally, curve D shows the effect of changing the orbital reduction parameter $k$ from 1.0 to 0.5. Not only has the room-temperature $\mu_{eff}$ decreased from ~4.6 to 4.2 BM, but the curve is fairly flat to ~30°K, a reflection of a much smaller zero-field splitting.

It should be pointed out that for the standard curves plotted in Figure 7 the range of room-temperature $\mu_{eff}$ values of 4.2–4.6 BM is considerably above the spin-only value for a quartet ground state (3.87 BM). This is due to two major effects. The first of these is spin–orbit coupling which mixes the $^4A_2'$ ground state with the $^4E''$ excited state, as pointed out above, and the second is the mixing of the $^4A_2'(F)$ ground state with the higher-energy $^4A_2'(P)$ state via the $D_{3h}$ crystal field operator. Both of these mechanisms are effective in increasing the net magnetic moment of the ground state. The contributions of each of these mechanisms to the curvature of the $\mu_{eff}$ curve at low temperatures are potentially different, and it will be shown below that the simultaneous consideration of both effects is necessary in order to fit correctly the observed data for a monomeric system.

The calculation of TIP is an essential preliminary to any quantitative fit of magnetic susceptibility data for cobalt(II) systems. Basically we are concerned with second-order Zeeman coupling of excited states to the ground state, where these excited states cannot be thermally populated. The application of the $H_x$ Zeeman operator

$$\bar{H}_x = [(kL_+ + kL_-) + (S_+ + S_-)]H_x$$

to the $|^4E''\ 3, \pm1, {}^3/_2, {}^3/_2\rangle$ wave function illustrates that the following nonzero matrix element may be found

$$\langle {}^4A_2'\ 3, 0, {}^3/_2, {}^3/_2 | H_x | {}^4E''\ 3, \pm1, {}^3/_2, {}^3/_2\rangle = \sqrt{3}k\beta H_x$$

Using second-order perturbation theory, the change in energy of the $^4A_2'$ states as a consequence of this effect may be written

$$E' = 3k^2H_x^2/\Delta E$$

where $\Delta E = E(^4A_2') - E(^4E'')$. Calculation of the susceptibility component of this term contributed to all four $^4A_2'$ levels yields $\chi_{TIP} = 12N\beta^2k^2/\Delta E$.

The effects of spin–orbit coupling, $^4A_2'(F)$–$^4A_2'(P)$ mixing, and TIP may all be studied by reference to Figure 8. Here the observed magnetic susceptibility data for [Co(Me$_6$tren)Cl]Cl have been plotted (as $\mu_{eff}$) along with the results of fittings (solid lines) to the data with various parameters. In the first place, note the lower temperature region of the figure. For solid curve A, where no spin–orbit coupling is allowed, only $^4A_2'(F)$–$^4A_2'(P)$ mixing contributes to the magnetic moment (that is, above spin only, ignoring TIP for now). The parameters given for curve A have been adjusted for minimum error from the experimental data, although it is clear that while the room-temperature moment can be duplicated, the low-temperature curvature is completely wrong. Curve C, where only spin–orbit coupling is allowed, can also fit the room-temperature data, but the large $k$ value required causes the $(\pm{}^3/_2)$–$(\pm{}^1/_2)$ Kramers doublet splitting to be large and thus the moment would be predicted to decrease greatly at lower temperatures, much more than observed experimentally for the monomeric system. When *both* $^4A_2'(F)$–$^4A_2'(P)$ mixing and spin–orbit coupling are included in the calculation, the curvature in the low-temperature range of the $\mu_{eff}$ curve may be duplicated very closely, certainly to within experimental error (see Figure 8 and Table IV[17]). The good correspondence tends to confirm both the monomeric nature of the molecule and the essential correctness of our mathematical model.

At higher temperatures the fitting of the monomer susceptibility equations to the observed data is very much dependent upon the TIP contribution, whereas this effect is negligible below 60°K. In general it will be assumed that $\chi_{TIP} \simeq 0.0002$ cgsu. The best value for the TIP in order to fit the [Co(Me$_6$tren)Cl]Cl data would appear to be ~0.00015, which is close to the 0.00017 calculated theoretically on the basis of $\Delta E = 5800$ cm$^{-1}$ and $k = 0.56$. Table IV[17] lists the observed and calculated magnetic data for the Me$_6$tren monomer with the best final set of parameters; these parameters give $D \simeq 10$ cm$^{-1}$.

The small size of $k$ for the fitting to the cobalt monomer data raises some concern, as it is generally considered that 0.8–0.9 is normal for similar systems, and Wood[19] suggested that $k$ for this same material is near 1.0 on the basis of room-temperature magnetic data (he did not, however, include a $^4A_2'(F)$–$^4A_2'(P)$ mixing term in his calculations). No attempt will be made to rationalize the size of $k$. Irrespective of the precise fit of the model to both the electronic spectra and susceptibility of [Co(Me$_6$tren)Cl]Cl, the important point is that the low-temperature magnetic data can be fit well for a monomeric compound with a monomeric crystal field model. It then remains to be seen whether the $[Co_2(tren)_2X_2](BPh_4)_2$ species will give susceptibility data that can or cannot be fit by this same model. Any inconsistencies at low temperature may be taken as indications of exchange interactions.

Figure 9 and Table V[17] show the results of fitting the magnetic data for $[Co_2(tren)_2(NCO)_2](BPh_4)_2$ and $[Co_2(tren)_2(N_3)_2](BPh_4)_2$ with the $D_{3h}$-symmetry monomer model, i.e., model A. For the cyanate the fit is good throughout most of the temperature range, although at low temperatures (<10°K) the experimental $\mu_{eff}$ values fall below those calculated, $\mu_{eff}$(exptl) = 3.35 BM and $\mu_{eff}$(calcd) = 3.48 BM at 4.2°K. More noticeable is the disparity in the sub-10°K range for the azide complex, where the lowest observed moment is 2.92 BM and the lowest calculated value is 3.59 BM. All in all, the presence of weak exchange interactions is suggested with that for the azide being stronger than that for the cyanate. The least-squares fitting parameters are as follows: cyanate, $k = 0.70$, $Ds = 968$ cm$^{-1}$, $Dt = 1600$ cm$^{-1}$, $\Delta = 11{,}670$ cm$^{-1}$; azide, $k = 0.85$, $Ds = 371$ cm$^{-1}$, $Dt = 1903$ cm$^{-1}$, $\Delta = 11{,}670$ cm$^{-1}$.

Observed and calculated susceptibility data for $[Co_2(tren)_2Cl_2](BPh_4)_2$ are given in Table VI[17] and it is found that the data can be quite adequately fit with model A to give parameters similar to those for [Co(Me$_6$tren)Cl]Cl. Therefore, no evidence is found to implicate an exchange interaction in the Co–tren–Cl compound. This is an interesting observation

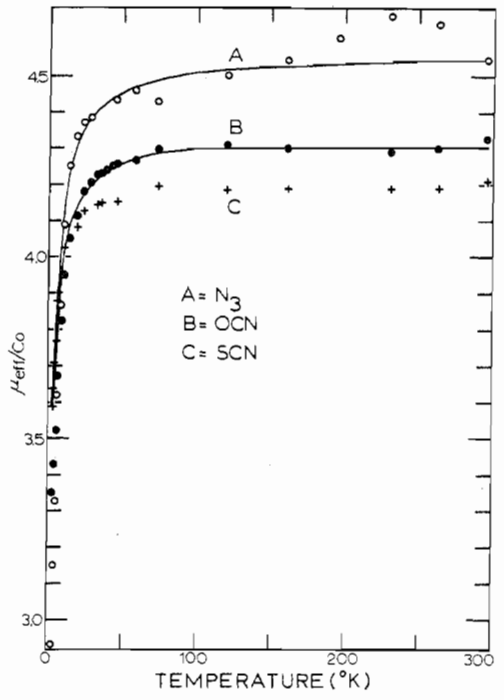


Figure 9. Variable-temperature effective magnetic moment data and $D_{3h}$ monomeric expression least-squares fitting results for $[Co_2(tren)_2X_2](BPh_4)_2$ where $X^- = N_3^-$ (A), $OCN^-$ (B), and $SCN^-$ (C). No fitting was attempted for the thiocyanate data in that they were not well determined on an absolute scale. The lowest values of $\mu_{eff}$ reached by the theoretical lines represent the calculated values at the lowest experimental temperature (i.e., 4.2°K).

in that, as far as the Cu–tren outer-sphere dimer series is concerned, $[Cu_2(tren)_2Cl_2](BPh_4)_2$ exhibits one of the largest interactions with $J = -3.2$ cm$^{-1}$ (antiferromagnetic).[11,12] The suggestion that the Co–tren chloride compound should really be formulated as monomeric [Co(tren)Cl](BPh4) will be countered in the following EPR section.

Referral to Tables V[17] and VI[17] shows that for these cobalt azide, cyanate, and chloride compounds there are large variations in $k$ from the susceptibility fittings and this is understandable in that this parameter is of the greatest importance in determining the zero-field splitting. With $k = 0.85$ for the azide system, the $(\pm 3/2)$–$(\pm 1/2)$ splitting is $\sim$29 cm$^{-1}$, an increase by a factor of 3 over what was found for [Co(Me6tren)Cl]Cl. It is unlikely that this really reflects such an increased single-ion zero-field splitting in the azide. It is suggested that the fitting procedure is using a large zero-field splitting to account for exchange coupling which is present and exchange coupling for which we have not to this point allowed.

Variable-temperature magnetic susceptibility data were also collected for $[Co_2(tren)_2(NCS)_2](BPh_4)_2$ (see Figure 9). Because an accurate absolute room-temperature $\mu_{eff}$ was not obtained for this compound, the data are not reported. Moreover, by assuming a reasonable room-temperature $\mu_{eff}$ it is found that the effective moment decreases only as much with decreasing temperature as would be expected on the basis of zero-field splitting. Therefore, as in the chloride case no evidence for exchange is found.

Thus, for the series of $[Co_2(tren)_2X_2](BPh_4)_2$ compounds where $X^- = OCN^-$, $Cl^-$, and $N_3^-$, the ordering of 4.2°K magnetic moments is $N_3^- < OCN^- < Cl^-$ and the model A monomer equations give the poorest fit for the azide implicating an exchange interaction. For these reasons and because of the calculational cost, only the azide data have been carefully fit to the model B dimer equations which with an effective spin Hamiltonian take into account an isotropic exchange interaction and single-ion zero-field splitting. Before the results of this fitting are discussed, it is beneficial to investigate empirically the effects of changing one or more of the parameters ($J$, $g_\perp$, $g_\parallel$, and $D$) of model B. The $g$ values have been selected for this illustration as equal to those reported[30] for [Co(Me6tren)Cl]Cl, $g_\parallel = 2.29$ and $g_\perp = 4.25$. We have found (see Figure 10) that for various values of $J$ and $D$ the value of $J$ has the greatest effect in decreasing the low-temperature magnetic moment. For $D = -5$ cm$^{-1}$, which corresponds to a $(\pm 3/2)$–$(\pm 1/2)$ single-ion splitting of 10 cm$^{-1}$ as found for [Co(Me6tren)Cl]Cl, it is only through the presence of exchange coupling that 5°K moments below 3.5 BM are obtained.

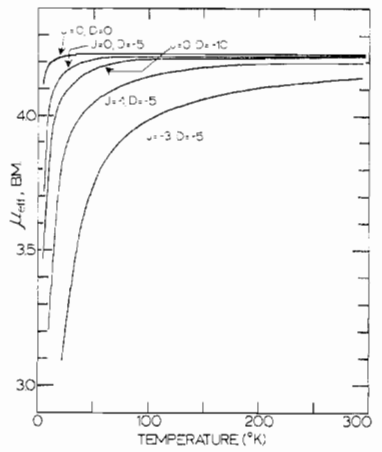


Figure 10. Magnetic moment curves calculated using the $S_1 = S_2 = 3/2$ dimer susceptibility expression which includes a single-ion zero-field interaction ($D$). The choice of parameters in cm$^{-1}$ is indicated in the figure.

One check of the model B machinery was made by recasting the [Co(Me6tren)Cl]Cl data in terms of a dimer (i.e., double the measured monomer susceptibility values) and subjecting these data to a fit with model B where $J$ is fixed as zero, and $g_\perp$, $g_\parallel$, and $D$ were all varied for best agreement. The zero-field parameter $D$ was taken as negative to ensure that the $\pm 1/2$ Kramers doublet is lowest in energy. With the values $J = 0$, $g_\parallel = 2.215$, $g_\perp = 4.486$, and $D = -5.13$ cm$^{-1}$ (TIP for the "dimer" was fixed at 0.0003 cgsu) an excellent fit to the data was obtained. As can be seen in Table VII[17] the observed–calculated agreement is better than 0.7% at all but one low-temperature point. It is notable that the $g$ values are similar to those reported for this compound and most importantly, the effective $(\pm 3/2)$–$(\pm 1/2)$ splitting is 10.3 cm$^{-1}$, which is well in accord with that found by fitting the same data to model A for a $D_{3h}$ symmetry monomer.

The results of fitting the $[Co_2(tren)_2(N_3)_2](BPh_4)_2$ data to model B are illustrated in Figure 11 and are given in Table VIII.[17] As would be expected, the inclusion of the exchange term allows a much improved fit to the azide susceptibility data than was possible with the monomer model A. Although there is considerable scatter in the higher temperature points, the curve is, on the average, fit well and the calculated $J$ value of –0.50 cm$^{-1}$ (antiferromagnetic interaction) is, in our opinion, likely to be reasonably accurate, particularly considering the "sensitivity" of total spin $S' = 3$ $J$ values. Unfortunately, we cannot give correlation errors between the various parameters in this fitting. The $g$ values ($g_\perp = 4.81$ and $g_\parallel = 2.18$) obtained for the fit are somewhat different from those observed for [Co(Me6tren)Cl]Cl ($g_\perp = 4.476$ and $g_\parallel = 2.423$) and the zero-field splitting ($D = -5.0$ cm$^{-1}$) is comparable to that for the chloride monomer. The zero-field splitting is not expected to be as strong a function of the bridging anion as is $J$. However, it is interesting to note that $D$ does not follow the change in $g$ values from the Me6tren–Cl to the tren–$N_3$

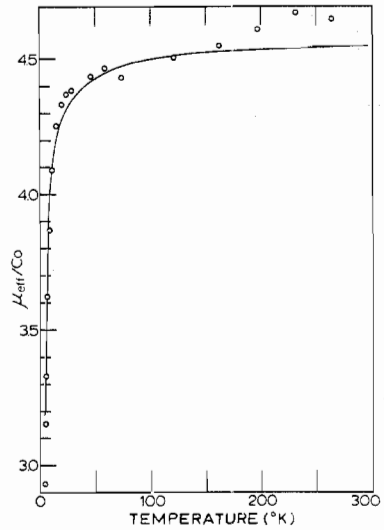


Figure 11. Fitting of the observed susceptibility data for $[Co_2(tren)_2(N_3)_2](BPh_4)_2$ to the $S' = 3$ dimer expression; for fitting parameters see text.

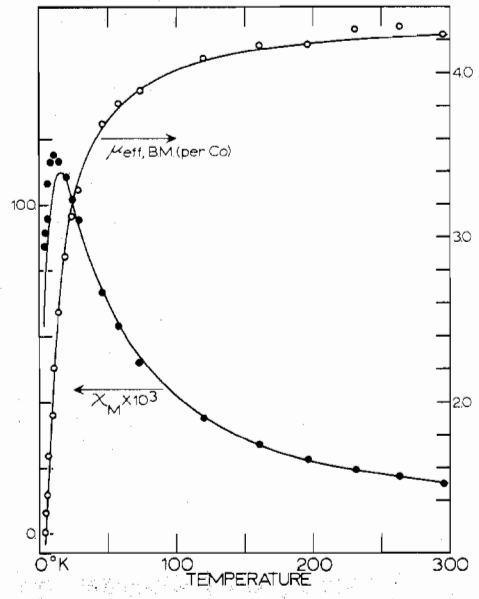


Figure 12. Molar susceptibility (cgsu/mol of dimer) and effective magnetic moment data for $[Co_2(tren)_2Ox](BPh_4)_2$. The lines are least-squares theoretical fittings using a $S_1 = S_2 = 3/2$ isotropic exchange dimer expression where single-ion zero-field interactions are ignored.

compound. It may be that in this case the changes in $g$ values are reflecting a change in geometric distortion.

The magnetic susceptibility data for $[Co_2(tren)_2Ox](BPh_4)_2$ are presented in Table IX[17] and Figure 12, and the presence of a magnetic exchange effect is clearly noticeable in that the $\chi_M$ vs. temperature curve peaks at ~10°K. In view of the work of Lines[8] on exchange between $^4T$ ground-state systems, an attempt was made to incorporate the Lines equations into a fitting program. Although the details of the procedure were carefully carried out and checked several times, the expressions used would not give reasonable susceptibility values for the parameters used and no fitting was done with the Lines theory. The more recent work of Ball and Blake[7] has been of use, however. They discussed the fitting of susceptibility data for octahedral cobalt(II) dimers, both with and without consideration of orbital angular momentum effects. Because they do not list the matrix elements used for the calculation of the susceptibility for the "complete" orbital scheme, it was not possible to fit our data to their equations. However, they do compare the results of a "spin-only" (i.e., simply $-2JS_1 \cdot S_2$) approach with the results obtained considering an orbital contribution and it was found that in general (five out of six compounds studied) the ratio of $J$ for the spin-only approach to $J$ for the orbital picture is 1.37 ± 0.05. The overestimation of $J$ by using the spin-only picture is expected in that $J$ is to a large extent used to account for zero-field splitting of the $^4T$ ground state, as well as for exchange effects.

Fitting of the magnetic susceptibility data for the oxalate compound with model C which uses the "spin-only" equations yields the theoretical fit and parameters indicated in Table IX[17] and Figure 11. The parameters obtained are $J = -3.09$ cm$^{-1}$, $g = 2.21$, and $\Theta = -1.3°$. Applying the above correction factor gives $J_{cor} \simeq -2.2$ cm$^{-1}$. It is seen from Figure 11 that the peak has been only poorly fit; perhaps the functionality of the spin-only equation is not quite proper, but it is clear that $J$ for this oxalate compound lies in the range between −1 and −3 cm$^{-1}$.

Previously we reported that $J = -16$ cm$^{-1}$ for $[Ni_2(tren)_2Ox](BPh_4)_2$.[31] As pointed out by Ball and Blake[7] the ratio of $J_{Ni}/J_{Co}$ should be $9/4$ if no orbital effects are present. For their series of dimers the value of $4J_{Ni}/9J_{Co}$ was found to be 1.9 ± 0.3. If we calculate this number for our tren oxalate dimers, we find that $4J_{Ni}/9J_{Co} \geq 2.3$. Following their discussion it may be concluded that the extra $t_{2g}$ electron in the cobalt system is involved in an exchange pathway that is ferromagnetic.

In summary, it appears that variable-temperature magnetic susceptibility for the Co$^{II}$–tren compounds can only give qualitative indications and/or semiquantitative assessments of the extent of exchange interactions. Clear indications of the associated nature of the Co(II) centers in these compounds and potentially accurate determinations of $J$ can be obtained from EPR measurements, to which we turn.

**Electron Paramagnetic Resonance.** There are two aspects of dimeric Co(II) systems that can lead to complicated EPR observations, one being the presence of exchange coupling which, in conjunction with the small single-ion zero-field splitting, results in an arrangement of the 16 dimer energy levels such that there are transitions between the various Zeeman-split manifolds. Second, the proximity of the metal ions leads to large through-space dipolar zero-field splitting which is orientation dependent. This latter term will not be energetically large relative to the overall spread of energies encountered for a system but will split apart the most important levels (with respect to observation by EPR) and result in obvious changes in the spectra. It cannot really be assumed that the general spectrum can be assigned without inclusion of the interion zero-field splitting term. Needless to say, simulation of a powder spectrum of a high-spin cobalt(II) dimer under conditions where the Zeeman energies, exchange interactions, and single-ion zero-field interactions are of comparable magnitude (folding in interion zero-field terms) requires an exact treatment (i.e., diagonalization of matrices as opposed to a perturbation treatment). Such an endeavor is only of late economically feasible with the approach set out by Belford and Belford.[32] Work has been initiated in these laboratories to simulate our spectra, but for the present we will have to be happy with a reporting of the spectra and a qualitative discussion.

The reported[30] spectrum of $[Co(Me_6tren)Cl]Cl$ is quite simple in appearance; the spectrum is axial and independent of temperature from 90 to 4.2°K with $g_\parallel = 2.29$ and $g_\perp = 4.25$. There are only the two simple features to be seen in the spectrum, and they are interpreted as transitions within the $\pm 1/2$ monomer Kramers doublet, where with no spin–orbit coupling the $g$ values may be shown to be $g_\parallel = 2.0$ and $g_\perp = 4.0$.

The ~12°K X-band EPR spectra of $[Co_2(tren)_2X_2]$-

Table X. Q-Band EPR Data for $[Co_2(tren)_2X_2](BPh_4)_2$

| $X^- = Cl^-$ | | | $X^- = NCS^-$ | | | $X^- = N_3^-$ | | | $X^- = NCO^-$ | | |
|---|---|---|---|---|---|---|---|---|---|---|---|
| Label | $H$[a] | $g$ | Label | $H$ | $g$ | Label | $H$ | $g$ | Label | $H$ | $g$ |
| | | | | | | $L_1$ | 635 | | $L_1$ | ~0 | |
| $L_1$ | 2,480 | 10.1 | $L_1$ | 3,192 | 8.17 | $L_2$ | 2,220 | | $L_2$ | 7,520 | 3.47 |
| $L_2$ | 3,050 | 8.20 | | | | $L_3$ | 3,970 | 6.30 | $L_3$ | 12,120 | 2.15 |
| $L_3$ | 5,190 | 4.82 | $L_2$ | 4,575 | 5.70 | | | | $L_4$ | 13,300 | 1.96 |
| $L_4$ | 12,970 | 1.93 | $L_3$ | 12,235 | 2.13 | $L_4$ | 9,950 | 2.51 | | | |
| | | | $L_4$ | (14,900) | 1.75 | | | | | | |
| | | | | | | $H_1$ | 1,376 | | | | |
| $H_1$ | 4,850 | 5.16 | | | | $H_2$ | 4,550 | 5.50 | $H_1$ | 5,138 | 5.07 |
| $H_2$ | 8,330 | 3.00 | $H_1$ | 8,792 | 2.97 | $H_3$ | 8,940 | 2.80 | | | |
| $H_3$ | (10,730) | 2.33 | $H_2$ | 10,160 | 2.57 | $H_4$ | 13,490 | 1.85 | | | |

[a] All fields given in gauss.

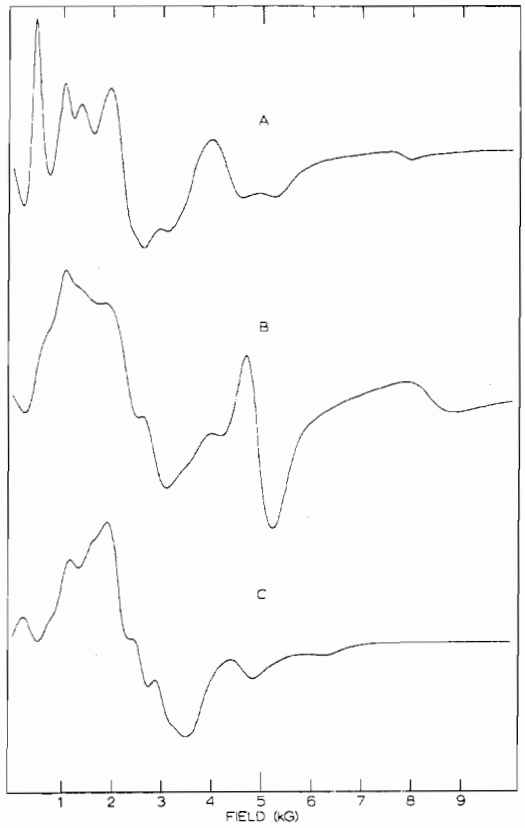


Figure 13. X-Band (~12°K) EPR spectra for $[Co_2(tren)_2X_2](BPh_4)_2$ where $X^- = N_3^-$ (A), $OCN^-$ (B), and $SCN^-$ (C). All samples were run as powders.

$(BPh_4)_2$, where $X^- = N_3^-$ (A), $NCO^-$ (B), and $NCS^-$ (C), are reproduced in Figure 13. The spectra are amazingly complicated! It is the obvious difference between these spectra and that for the structurally and almost even magnetically similar $Me_6$tren complex that supports so strongly the case for the tren compounds being formulated as dimers.

It was thought that in order to have any likelihood of interpretating these spectra in detail it would be necessary to have more highly resolved features—and this plus an advantageous "sorting" effect can be achieved by recording the spectra with higher microwave energies. Whereas the X-band spectra were all recorded at ~12°K, Q-band spectra were obtained at both 4.2 and ~90°K. Figure 14 shows the Q-band results for $[Co_2(tren)_2Cl_2](BPh_4)_2$ and it is clear that the complexity of the spectra establishes the dimeric nature of this compound. The temperature dependence should be of considerable help in assigning features; Table X lists the $g$ values from the high- and low-temperature Q-band spectra of all four compounds ($N_3^-$, $NCO^-$, $NCS^-$, and $Cl^-$). It can be seen in Figure 14 that the peaks labeled $L_1$, $L_2$, $L_3$, and $L_4$ seem to

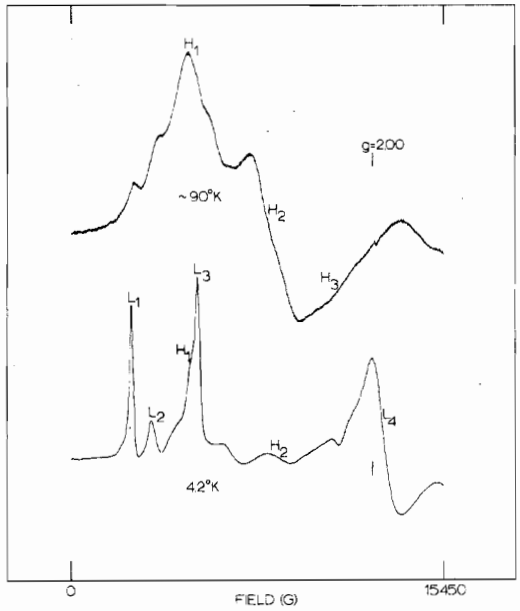


Figure 14. Q-Band EPR spectra of a powdered sample of $[Co_2(tren)_2Cl_2](BPh_4)_2$ at two temperatures.

remain as strong at 4.2°K as they are at ~90°K, or stronger. This implies that they occur within the lowest manifold of the system. It would be attractive to call $L_1$ and $L_3$ two interion zero-field split components of the $g_\perp$ transition where $2D_\perp$ = 570 G. This could only be checked by knowing the Co–Co distance and the relative **g–D** tensor orientation. A discussion of **g–D** tensor orientation effects for copper dimers is presented in the next paper in this series.[33] The $L_4$ signal is probably the parallel signal from the lowest manifold, broadened by a small parallel zero-field splitting. $H_1$ and $H_2$ are two bands that *appear* to be parallel and perpendicular components from some higher energy manifold. It is not possible at present to understand confidently the gross features of the chloride X-band spectrum, but it does appear that the features in the 4.2°K Q-band spectrum are at least tentatively assignable.

In passing it should be mentioned that a unique observation has been made with respect to the power saturation of peaks for the chloride EPR spectrum. By adjusting the power level the observed peaks are made to change in intensity and sometimes "flip over", each peak doing so *ostensibly* independent of the other peaks. As a result very differently appearing spectra can be obtained at higher power settings; the reported spectra are the low-power limiting spectra.

The compound $[Co_2(tren)_2(NCS)_2](BPh_4)_2$ gives rise to Q-band spectra (see Figure 15) that are similar to those for the chloride and as such the 4.2°K features are interpretable on the basis of interion zero-field splitting. We tentatively suggest that for the 4.2°K spectrum the two peaks at low field ($L_1$ and $L_2$) are zero-field split $g_\perp$ bands, while the two

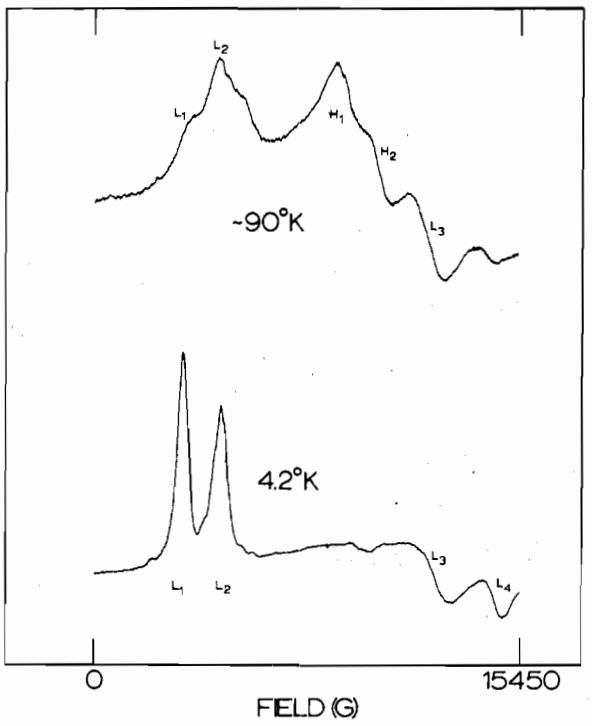


Figure 15. Q-Band EPR spectra of a powdered sample of $[Co_2(tren)_2(NCS)_2](BPh_4)_2$ at two temperatures.

high-field transitions ($L_1$ and $L_4$) are the zero-field split parallel signals. As above, these transitions all originate in the low-energy manifold and the additional peaks in the ~90°K spectrum have clear analogies in the chloride case. It is interesting to note the *average* of the positions of peaks $L_1L_2$ in the thiocyanate spectrum is the same for the average in the chloride spectrum. The splitting is larger for the chloride and if these splittings are indeed due to dipole–dipole interactions and the **g**–**D** tensor orientation does not change, then the metal–metal distance is clearly smaller for the chloride compound.

The Q-band spectra for the cyanate compound are given in Figure 16. It is intriguing that the peak labeled $L_1$ is close to 0, corresponding to a transition between two levels separated at zero-field by exactly the Q-band microwave energy. The larger zero-field interaction required by assigning $L_1$ and $L_2$ as the zero-field split perpendicular signals could result from a small Co–Co distance or a change in the orientation between the **g** and **D** tensors. With this assignment, the $L_3$ and $L_4$ features are the zero-field split parallel transitions. It is necessary to have the structure and single-crystal EPR data for this cyanate compound to eliminate an alternative assignment of peaks $L_2$, $L_3$, and $L_4$ to the $g_x$, $g_y$, and $g_z$ transitions from the lowest energy level (no zero-field splitting). In this case $L_1$ would result from an interlevel essentially zero-field transition.

The Q-band EPR spectra of $[Co_2(tren)_2(N_3)_2](BPh_4)_2$ were recorded as shown in Figure 17. In addition to a relatively large copper impurity signal at $g \simeq 2$ there are a considerable number of peaks. The peaks labeled $H_2$, $H_3$, and $H_4$ appear to be a $g_x$, $g_y$, and $g_z$ pattern from some higher lying manifold of the system, while $L_1$, $L_2$, $L_3$, and $L_4$ can be assigned to the ground manifold. Until (*and if*) simulations are possible, we will refrain from assigning these features in detail.

## Conclusion

The compound $[Co_2(tren)_2Ox](BPh_4)_2$ has a cation that consists of two octahedrally coordinated high-spin Co(II) ions bridged by a bis-bidentate oxalate moiety. A weak antiferromagnetic exchange with $J$ in the range of $-1$ to $-3$ cm$^{-1}$ has been found. Very weak (i.e., $J$ in the range of 0 to $-0.5$ cm$^{-1}$) antiferromagnetic interactions have been found via magnetic susceptibility for the $[Co_2(tren)_2X_2](BPh_4)_2$ compounds where $X^- = Cl^-$, $N_3^-$, $NCO^-$, and $NCS^-$. Infrared and electronic measurements clearly point to trigonal-bipyramidal Co(II) centers in these compounds, and this taken with the complicated EPR spectra shows that these compounds have cations that are dimeric by virtue of some outer-sphere association (for example hydrogen bonding).

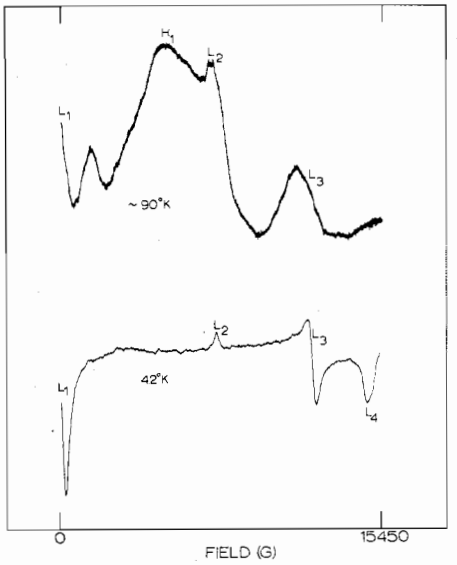


Figure 16. Q-Band EPR spectra of a powdered sample of $[Co_2(tren)_2(NCO)_2](BPh_4)_2$ at two temperatures.

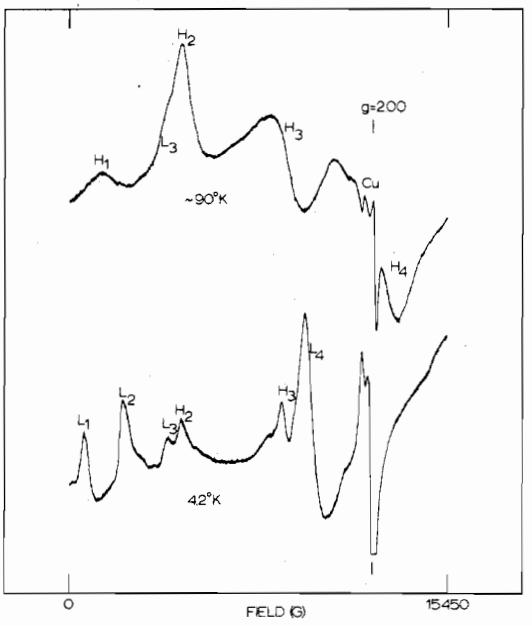


Figure 17. Q-Band EPR spectra of a powdered sample of $[Co_2(tren)_2(N_3)_2](BPh_4)_2$ at two temperatures; note the relatively large copper signal.

**Acknowledgment.** We are grateful for partial funding of this research by National Institutes of Health Grant HL 13652 and for discussions with Professor R. L. Belford. The Varian Model E-9 EPR spectrometer was purchased, in part, by a National Science Foundation departmental instrument grant.

**Registry No.** $[Co_2(tren)_2Cl_2](BPh_4)_2$, 55190-92-6; $[Co_2(tren)_2(NCS)_2](BPh_4)_2$, 55252-87-4; $[Co_2(tren)_2(N_3)_2](BPh_4)_2$, 55190-94-8; $[Co_2(tren)_2(NCO)_2](BPh_4)_2$, 55190-96-0; $[Co_2(tren)_2(C_2O_4)](BPh_4)_2$, 55190-98-2.

**Supplementary Material Available.** Tables I, II, and IV–IX, showing analytical data, relevant ir bands, and magnetic susceptibility data, will appear following these pages in the microfilm edition of this volume of the journal. Photocopies of the supplementary material from this paper only or microfiche (105 × 148 mm, 24× reduction, negatives) containing all of the supplementary material for the papers in this issue may be obtained from the Journals Department, American Chemical Society, 1155 16th St., N.W., Washington, D.C. 20036. Remit check or money order for $4.50 for photocopy or $2.50 for microfiche, referring to code number AIC40741N.

## References and Notes


(1) Esso Fellow, 1971–1972; Mobil Fellow, 1972–1973; University of Illinois Fellow, 1973–1974.
(2) Camille and Henry Dreyfus Fellow, 1972–1977.
(3) G. A. Rodley and W. T. Robinson, *Nature (London)*, **235**, 438 (1972), and references therein.
(4) C. Busetto, F. Cariate, A. Fusi, M. Gullotti, F. Morazzoni, A. Pasini, R. Ugo, and V. Valenti, *J. Chem. Soc., Dalton Trans.*, 754 (1973).
(5) R. Morassi, I. Bertini, and L. Sacconi, *Coord. Chem. Rev.*, **11**, 343 (1973), and references therein.
(6) P. W. Ball and A. B. Blake, *J. Chem. Soc., Dalton Trans.*, 852 (1974).
(7) P. W. Ball and A. B. Blake, *J. Chem. Soc. A*, 1415 (1969).
(8) M. E. Lines, *J. Chem. Phys.*, **55**, 2977 (1971).
(9) D. M. Duggan, R. G. Jungst, K. R. Mann, G. D. Stucky, and D. N. Hendrickson, *J. Am. Chem. Soc.*, **96**, 3443 (1974); D. M. Duggan and D. N. Hendrickson, *Inorg. Chem.*, **13**, 1911 (1974).
(10) D. M. Duggan and D. N. Hendrickson, *Inorg. Chem.*, **13**, 2929 (1974).
(11) E. J. Laskowski, D. M. Duggan, and D. N. Hendrickson, unpublished results.
(12) D. M. Duggan and D. N. Hendrickson, "Extended Interactions between Transition Metal Ions", L. Interranti, Ed., American Chemical Society Symposium Series, No. 5, Washington, D.C., 1974.
(13) G. A. Barclay and A. K. Barnard, *J. Chem. Soc.*, 2540 (1958).
(14) P. Paoletti, M. Ciampolini, and L. Sacconi, *J. Chem. Soc.*, 3589 (1963).
(15) I. Bertini, M. Ciampolini, and D. Gatteschi, *Inorg. Chem.*, **12**, 693 (1973).
(16) M. Di Vaira and P. L. Orioli, *Inorg. Chem.*, **6**, 955 (1967).
(17) Supplementary material.
(18) M. Ciampolini and N. Nardi, *Inorg. Chem.*, **5**, 41 (1966).
(19) J. S. Wood, *Inorg. Chem.*, **7**, 852 (1968); J. S. Wood, *J. Chem. Soc. A*, 1582 (1969).
(20) J. S. Wood, *Prog. Inorg. Chem.*, **16**, 227 (1972).
(21) D. Gatteschi and I. Bertini, Abstracts, Third National Meeting of the Italian Association of Inorganic Chemists, 1970, No. C34, and unpublished results.
(22) E. J. Laskowski and D. N. Hendrickson, unpublished results.
(23) D. M. Duggan and D. N. Hendrickson, *J. Chem. Soc., Chem. Commun.*, 411 (1973).
(24) D. M. Duggan and D. N. Hendrickson, *Inorg. Chem.*, **13**, 2056 (1974).
(25) C. G. Pierpont, D. N. Hendrickson, D. M. Duggan, F. Wagner, and E. K. Barefield, *Inorg. Chem.*, **14**, 604 (1975).
(26) C. Postmus, J. R. Ferraro, A. Quattrochi, K. Shobatake, and K. Nakamoto, *Inorg. Chem.*, **8**, 1851 (1969).
(27) M. J. Norgett, J. H. M. Thornley, and L. M. Venanzi, *J. Chem. Soc. A*, 540 (1967).
(28) M. Ciampolini and I. Bertini, *J. Chem. Soc. A*, 2241 (1968).
(29) A. D. Liehr, *J. Phys. Chem.*, **67**, 1314 (1963).
(30) F. S. Kennedy, H. A. O. Hill, T. A. Kaden, and B. L. Vallee, *Biochem. Biophys. Res. Commun.*, **48**, 1533 (1972).
(31) D. M. Duggan, E. K. Barefield, and D. N. Hendrickson, *Inorg. Chem.*, **12**, 985 (1973).
(32) R. L. Belford, P. H. Davis, and G. G. Belford, 167th National Meeting of the American Chemical Society, Los Angeles, Calif., 1974, No. INOR 108.
(33) G. R. Hall, D. M. Duggan, and D. N. Hendrickson, *Inorg. Chem.*, in press.
(34) E. U. Condon and G. H. Shortley, "The Theory of Atomic Spectra", Cambridge University Press, London, 1959.


Contribution from the School of Chemical Sciences, University of Illinois, Urbana, Illinois 61801

# Magnetic Exchange Interactions in Transition Metal Dimers. V. Copper(II)–Diethylenetriamine Complexes with Oxalate, Cyanate, Thiocyanate, and Azide Inner- and Outer-Sphere Bridging Units. Electron Paramagnetic Resonance of Alkali Halide Pelleted Copper Complexes

GRETCHEN R. HALL,[1] D. MICHAEL DUGGAN,[2] and DAVID N. HENDRICKSON*[3]

*Received December 12, 1974* AIC40832K

Variable-temperature magnetic susceptibility and EPR are used to investigate compounds of the composition $[Cu_2(dien)_2X_2](BPh_4)_2$ where X = $Ox^{2-}/2$, $N_3^-$, $NCO^-$, and $NCS^-$ and dien is diethylenetriamine. The oxalate (Ox) compound is inner-sphere bridged wherein the oxalate is bis-bidentate. In contrast to $[Cu_2(dien)_2(Ox)](ClO_4)_2$ (X-ray structure is available) where no signs of an exchange interaction are seen in either the susceptibility to 4.2°K or the EPR spectrum, the susceptibility of $[Cu_2(dien)_2(Ox)](BPh_4)_2$ shows an antiferromagnetic interaction characterized by $J = -7.4$ cm$^{-1}$, $g = 2.16$, and $\Theta = 1.3°$ via least-squares fitting to the copper dimer equation. The structural changes of the dimeric cation required to account for this anion dependence are discussed. The weak ($|J| < \sim 0.5$ cm$^{-1}$) exchange interaction and relatively large zero-field splitting seen in the EPR of $[Cu_2(dien)_2(N_3)_2](BPh_4)_2$ are shown to be explicable in terms of a structure where two square-planar copper complexes are outer-sphere associated (hydrogen bonding) such that the Cu–Cu vector is normal to the copper coordination planes. Powdered-sample Q-band EPR spectra are computer simulated partially to substantiate this and the effects of Cu–Cu distance and **g** tensor–**D** tensor (i.e., Cu–Cu vector) orientation are illustrated for this azide as well as for $[Cu_2(dien)_2(Ox)](BPh_4)_2$. No exchange interactions are seen to 4.2°K in the susceptibility of $[Cu_2(dien)_2(NCO)_2](BPh_4)_2 \cdot 2H_2O$; however, the Q-band spectra of this compound and the analogous anhydrous thiocyanate compound give evidence of electron exchange; probable structures are proposed for the dimeric cations in these two compounds. EPR is used to study the effects on $[Cu_2(dien)_2(Ox)](ClO_4)_2$, which potentially has open copper coordination sites, of pelleting in KBr, KCl, KI, NaBr, and NaCl.

## Introduction

We have investigated[4–9] exchange interactions in the series $[Ni_2(tren)_2X_2](BPh_4)_2$, where tren is the tetraamine 2,2',2''-triaminotriethylamine and X = $Ox^{2-}/2$ (Ox = oxalate), $Sq^{2-}/2$ (Sq = squarate), $N_3^-$, $NCO^-$, $NCS^-$, and $NCSe^-$. These nickel(II) compounds have been shown[8–10] with X-ray crystallography to be dimeric with two X anions end-to-end bridging such that the nickel centers are octahedrally coordinated. It was found that it is the precise geometry of the bridging system in these nickel inner-sphere dimers that determines the sign (i.e., antiferromagnetic vs. ferromagnetic) and magnitude of the exchange interaction. Attempts to replace the nickel(II) atoms with copper(II) atoms in these tren compounds gave *outer*-sphere $[Cu_2(tren)_2X_2](BPh_4)_2$ ($X^-$ = $NCO^-$, $NCS^-$, $CN^-$, $Cl^-$, and $Br^-$) dimers where each copper center is trigonal bipyramidal and one end of the X group is hydrogen bonding to a tren nitrogen on the second copper center. The structural details of most of these interesting outer-sphere copper dimers[11–13] and two related outer-sphere manganese dimers,[14] $X^-$ = $NCS^-$ and $NCO^-$, have been determined by X-ray techniques.

In the present paper results are reported for a study of the